

Fluid flow and analyte diffusion in microfluidic devices
ECMI Modelling week 2008

Hermes Gadêlha, Siri-Malen Høyne,
Kjetil A. Johannessen, Xiangwen Kong,
Sean McGinty and Sudhir Srivastava

November 11, 2008

Contents

1	Introduction	1
1.1	Problem Formulation	1
2	The equations governing our system	4
2.1	Scaling	4
2.2	Boundary conditions	5
3	Analytic approach	7
3.1	Analytical solution of the fluid flow	7
3.2	Finding the concentration using perturbation-methods	8
4	Numerical computations	11
4.1	Finite difference discretization	11
4.2	Boundary Conditions	12
4.3	Grid, and construction of A	14
4.4	Results	14
5	The 2D advection-diffusion case	17
5.1	Approximate steady-state solution	17
5.2	Full numerical simulation	21
6	Conclusions	25

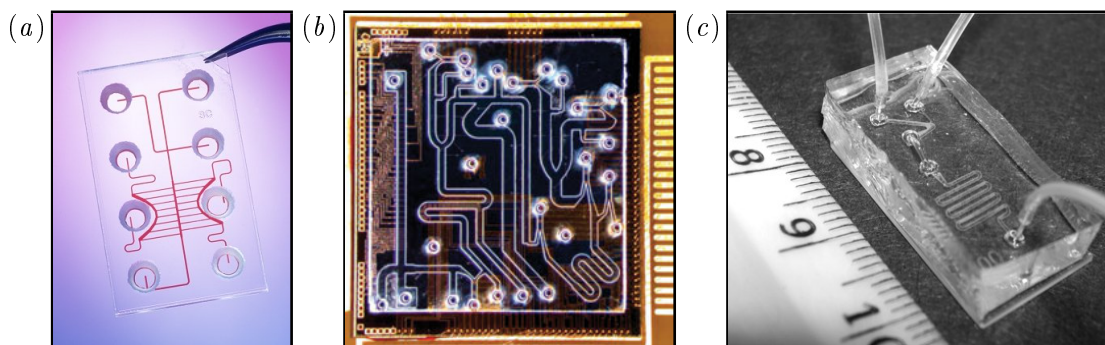


Figure 1: Several different microfluidic devices: (a) A chromosome sorter by Chung *et al.* (b) An integrated device for genetic analysis. (c) A continuous-flow device for detection of bacterial spores.

1 Introduction

Microfluidic devices are being used increasingly in industry for a wide variety of applications. Their small scale makes them suitable for cost effective high throughput testing and analysis, and as such they are ideal for biological applications such as cell analysis, immunoassays and DNA analysis. The commercially most successful application, however, is the inkjet printer.

As their name suggests, these devices are very small (often sub-millimetre), and contain fluid filled channels and chambers. Devices for biological applications are commonly constructed from Polydimethylsiloxane (PDMS), which can be poured as liquid onto a positive relief mold and cured using heat in such a way that channels are formed. Figure 1 shows several different microfluidic devices.

In this report, we look at one particular experimental design for a system to test the response of cells to differing concentrations of a specific analyte (substance). We devise a model and provide both an analytical and numerical treatment of the resulting equations to give useful insight into the problem.

1.1 Problem Formulation

The device under consideration has two main parts: the mixer and the interrogator. The solutions under test are fed into the mixer which consists of a network of small channels. The mixing is achieved by repeated splitting and recombining (by diffusion) of channels containing fluid of different concentrations. The solutions of different concentrations then reach the interrogator where they are passed over one or more cells. Analysis equipment is then used to determine the effect on the cells. The mixer region is beyond the scope of our work, and as such we assume that the concentrations and fluid velocity at the interrogator interface are known, allowing us to look solely at the interrogator. Figure 2 displays a plan-view sketch of the device being considered, while table 1 shows typical parameter values and ranges.

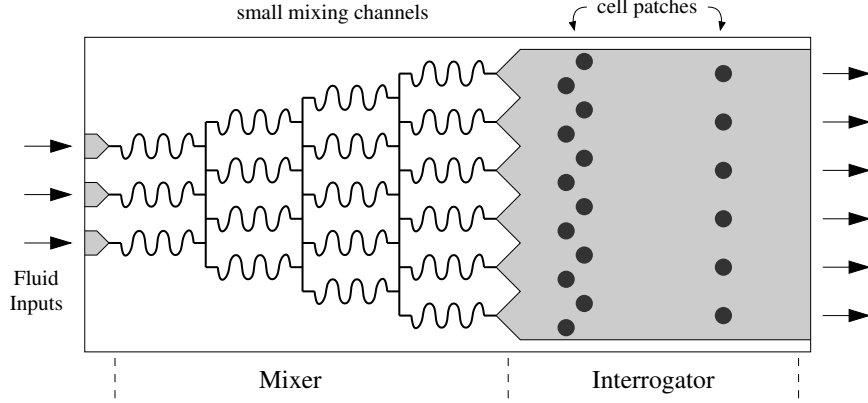


Figure 2: A plan-view sketch of the microfluidic device being considered.

Symbol	Parameter	Typical value	Units
H	depth of channels / chamber	$10^{-5} - 10^{-4}$	m
L	length of interrogator chamber	$10^{-2} - 10^{-1}$	m
W	width of interrogator chamber	$10^{-2} - 10^{-1}$	m
W_ℓ	lane width in interrogator	$\sim 10^{-2}$	m
W_m	channel width in mixer	$10^{-5} - 10^{-4}$	m
R_s	radius of cell patches	$\sim 5 \times 10^{-4}$	m
Q	volume flux (flow rate)	$10^{-12} - 10^{-10}$	$\text{m}^3 \text{s}^{-1}$
U	fluid velocity in interrogator	$\sim 10^{-5}$	m s^{-1}
D	diffusivity of analyte	$10^{-9} - 10^{-10}$	$\text{m}^2 \text{s}^{-1}$
c	concentration range	$10^{-10} - 10^{-4}$	mol m^{-3}
σ	cells receptor density	$10^{-9} - 10^{-8}$	mol m^{-2}
k	analyte uptake rate	$\sim 10^{-3}$	s^{-1}

Table 1: Typical parameter values and ranges.

In §2 we write down the governing equations and non-dimensionalize them. Then, in §3 we present an analytical solution of the fluid flow and use perturbation techniques on the concentration equation to show that the problem can be reduced to two dimensions. We then, in §4, devise a finite difference approximation for the three dimensional advection-diffusion equation before looking at the steady state solution of the two dimensional advection diffusion equation as well as the full numerical solution in §5. Finally we conclude our results in §6.

2 The equations governing our system

The equations we have been working with are the Navier–Stokes equations for an incompressible Newtonian fluid

$$\begin{aligned} \rho \left(\frac{\partial \tilde{\mathbf{u}}}{\partial \tilde{t}} + (\tilde{\mathbf{u}} \cdot \nabla) \tilde{\mathbf{u}} \right) &= -\nabla \tilde{p} + \mu \nabla^2 \tilde{\mathbf{u}} \\ \nabla \cdot \tilde{\mathbf{u}} &= 0 \end{aligned} \quad (1)$$

which describe the fluid flow $\tilde{\mathbf{u}}$ in the device, where \tilde{t} is the time, ρ is the fluid density, μ is the viscosity coefficient and \tilde{p} is the pressure in the fluid, and the advection–diffusion equation

$$\frac{\partial \tilde{c}}{\partial \tilde{t}} + (\tilde{\mathbf{u}} \cdot \nabla) \tilde{c} = D \nabla^2 \tilde{c} \quad (2)$$

describing the concentration \tilde{c} of analyte in the fluid, here D is the diffusivity of the concentration. All constants with approximated values tabulated in table 1.

2.1 Scaling

The first thing we did was to scale the equations to introduce dimensionless variables, each of size $\mathcal{O}(1)$. We here assumed, as before, a velocity field only flowing in the positive x -direction. The natural thing to do is to scale each lengthscale by the size of the box, and the velocity by the given approximate velocity strength U and the concentration by some unknown maximum concentration C . We then introduced the following scales.

$$\begin{aligned} \tilde{u} &= Uu \\ \tilde{c} &= Cc \\ \tilde{x} &= Lx \\ \tilde{y} &= Ly \\ \tilde{z} &= Hz \end{aligned} \quad (3)$$

This will now mean that our new dimensionless variables u, x, c, y and z are all dimensionless and $\mathcal{O}(1)$. In particular we have that u, x and z all contained within the interval $[0, 1]$. $y \in [0, a]$, where $a \in \mathcal{O}(1)$, to avoid being restricted to a square domain. As long as a is not too large (or small), then all of the following arguments will still hold. The beauty of the scaling for c is that we don't need at all to know what C is supposed to be, since this will anyway cancel out in the final equation. We just state that C is equal to whatever maximum concentration the system takes.

We inserted all scales into the concentration equation and rearranged the terms. The resulting advection-diffusion equation is then (assuming steady state)

$$\epsilon^2 P_e (\mathbf{u} \cdot \nabla) c = \epsilon^2 \left(\frac{\partial^2 c}{\partial x^2} + \frac{\partial^2 c}{\partial y^2} \right) + \frac{\partial^2 c}{\partial z^2} \quad (4)$$

where

$$\epsilon = \frac{H}{L}, P_e = \frac{UL}{D} \quad (5)$$

Realizing that $\epsilon = \frac{H}{L}$ is indeed small for our problem, the first thing that comes to mind, is to ignore all terms which includes ϵ . This gives the rise to the ordinary differential equation

$$\frac{\partial^2 c}{\partial z^2} = 0 \quad (6)$$

with the flux boundary condition (see section 4.2), ensuring that the solution is constant across the entire domain. However, this is a dangerously simplification to do, since we are ignoring the highest order derivative in both x and y direction. This means that we cannot satisfy as many boundary conditions as the problem dictates and the solution may be outright wrong.

What we instead did, was to implement the full scaled equation, and did several numerical experiments to map out the behaviour of our system.

One might also note that given our problem parameters for H, L, U and D tabulated in table 1, we have

$$\begin{aligned} \epsilon &\in \mathcal{O}(10^{-4}) \\ P_e &\in \mathcal{O}(10^4) \end{aligned} \quad (7)$$

2.2 Boundary conditions

We must have no slip conditions for the fluid flow at the top, bottom and the walls of the device, i.e.

$$\mathbf{u}|_{z=0} = \mathbf{0} \quad (8)$$

$$\mathbf{u}|_{z=1} = \mathbf{0} \quad (9)$$

$$\mathbf{u}|_{y=0} = \mathbf{0} \quad (10)$$

$$\mathbf{u}|_{y=1} = \mathbf{0}, \quad (11)$$

and we need no flux conditions for the concentration on the walls and on the top of the device. We have cells at the bottom of our device that are absorbing the analyte, hence in the areas with cells we need to have some flux of concentration at $z = 0$. This absorption is given by

$$\tilde{f}(\tilde{c}) = -\frac{D}{k\sigma} \frac{\partial \tilde{c}}{\partial \tilde{z}}.$$

This gives the boundary conditions

$$\left. \frac{\partial c}{\partial z} \right|_{z=0} = f(c) \quad (12)$$

$$\left. \frac{\partial c}{\partial z} \right|_{z=1} = 0 \quad (13)$$

$$\left. \frac{\partial c}{\partial y} \right|_{y=0} = 0 \quad (14)$$

$$\left. \frac{\partial c}{\partial y} \right|_{y=1} = 0 \quad (15)$$

for the advection–diffusion equation. If we are in an area without cells then $f(c) \equiv 0$.

3 Analytic approach

Before solving the problem numerically, it is important to get some information about how we expect our solutions to behave. First we will find an analytical solution to the equation where we have made some simplifications. Then we will use perturbation-methods to obtain a new set of equations which are easier to solve numerically, but still gives a good approximation to the solution.

3.1 Analytical solution of the fluid flow

We assumed that the velocity field was on the form $\tilde{\mathbf{u}} = u_1(\tilde{y}, \tilde{z})\hat{\mathbf{x}}$ and that the pressure was on the form $\tilde{p} = -\tilde{g}(\tilde{y}, \tilde{z})x$. The Navier–Stokes equation in this case is

$$\tilde{g}(\tilde{y}, \tilde{z}) + \mu \left(\frac{\partial^2 u_1}{\partial \tilde{y}^2} + \frac{\partial^2 u_1}{\partial \tilde{z}^2} \right) = 0 \quad (16)$$

$$\frac{\partial \tilde{g}}{\partial \tilde{y}} = 0 \quad (17)$$

$$\frac{\partial \tilde{g}}{\partial \tilde{z}} = 0, \quad (18)$$

where we have looked at the steady state. This shows us that the pressure \tilde{p} only depends on \tilde{x} , i.e. $\tilde{p} = -G\tilde{x}$, and the equation reduces to

$$\frac{\partial^2 u_1}{\partial \tilde{y}^2} + \frac{\partial^2 u_1}{\partial \tilde{z}^2} = -\frac{G}{\mu}. \quad (19)$$

Since the height of the box is much smaller than the width of the box it is natural to assume that the no-slip conditions on the bottom and top will affect the flow more than the no-slip conditions on the walls. So as a first approach to finding a solution we only considered the \tilde{z} -dependency and easily found the solution

$$u_1(\tilde{z}) = \frac{G}{2\mu} \tilde{z}(H - \tilde{z}). \quad (20)$$

Next we wanted to find the exact analytical solution to equation (19). We look for a solution $\tilde{u} = u_h + u_p$, where u_h satisfies

$$\frac{\partial^2 u_h}{\partial \tilde{y}^2} + \frac{\partial^2 u_h}{\partial \tilde{z}^2} = 0 \quad (21)$$

and u_p satisfies

$$\frac{\partial^2 u_p}{\partial \tilde{y}^2} + \frac{\partial^2 u_p}{\partial \tilde{z}^2} = -\frac{G}{\mu}. \quad (22)$$

By letting both u_h and u_p satisfy no-slip conditions at $\tilde{z} = 0$ and $z = H$ and put $u_h = -u_p$ at $\tilde{y} = 0$ and $\tilde{y} = W$, $u = u_h + u_p$ satisfy all no-slip conditions. The solution found in

equation (20) satisfies the no-slip condition at $\tilde{z} = 0$ and $\tilde{z} = H$, so it is a suitable u_p . Using separation of variables we then find the homogenous solution u_h to be

$$u_h(\tilde{y}, \tilde{z}) = \frac{G}{2\mu} \frac{8H^2}{\pi^3} \sum_{n \text{ odd}} \frac{1}{n^3} \frac{\cosh\left(\frac{n\pi}{H}\left(\tilde{y} - \frac{W}{2}\right)\right) \sin\left(\frac{n\pi}{H}\tilde{z}\right)}{\cosh\left(\frac{n\pi W}{2H}\right)}. \quad (23)$$

Our analytical solution to (19) is

$$\tilde{u}(\tilde{y}, \tilde{z}) = \frac{G}{2\mu} \left(\tilde{z}(H - \tilde{z}) + \frac{8H^2}{\pi^3} \sum_{n \text{ odd}} \frac{1}{n^3} \frac{\cosh\left(\frac{n\pi}{H}\left(\tilde{y} - \frac{W}{2}\right)\right) \sin\left(\frac{n\pi}{H}\tilde{z}\right)}{\cosh\left(\frac{n\pi W}{2H}\right)} \right), \quad (24)$$

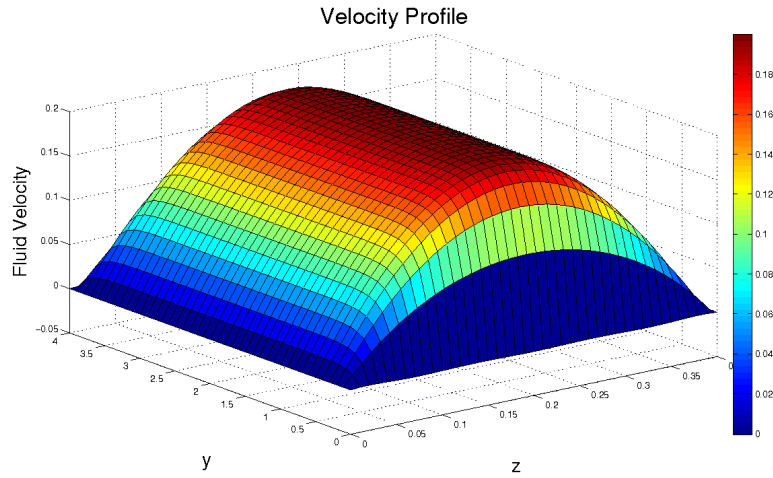


Figure 3: Plot of the solution (24), three terms in the sum included.

In figure 3 and 4 we see that the solution is constant in \tilde{y} in most of the box, so it looks like we might be able to neglect u_h . To see how good our first approximation was we calculate \tilde{y}_c , the critical distance from the walls where the \tilde{y} -dependent part has decreased to $p\%$ its maximum value. By Taylor expansion of the cosh we find

$$\tilde{y}_c \approx -\frac{H}{\pi} \ln \frac{p\pi^3}{6400}. \quad (25)$$

By choosing $p = 1\%$ we find $\tilde{y}_c \approx 1.7H$. Let us now put $\gamma = \frac{G}{2\mu}$.

3.2 Finding the concentration using perturbation-methods

We expand the concentration c as

$$c = c_0 + \epsilon^2(\bar{c}_1 + c'_1) + \epsilon^4(\bar{c}_2 + c'_2) + \mathcal{O}(\epsilon^6), \quad (26)$$

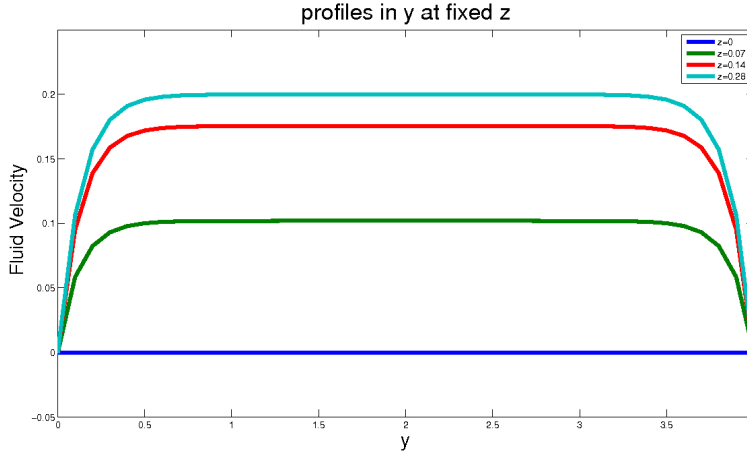


Figure 4: Plot of the solution (24) for fixed values of z , three terms in the sum included.

where we have $\bar{c}_i = \int_0^1 c_i dz$ such that $\int_0^1 c'_i dz = 0$. The splitting of c_i into \bar{c}_i and c'_i is motivated by (6). We assume here that $P_e \sim \mathcal{O}(1)$, only small modifications will be needed in the case where $P_e \approx \mathcal{O}(1)$. We insert this into equation (2), and by collecting terms of the same order we get

$$\epsilon^0 : \frac{\partial^2 c_0}{\partial z^2} = 0 \quad (27)$$

$$\epsilon^2 : P_e u \frac{\partial c_0}{\partial x} = \frac{\partial^2 c_0}{\partial x^2} + \frac{\partial^2 c_0}{\partial y^2} + \frac{\partial^2 c'_1}{\partial z^2} \quad (28)$$

$$\epsilon^4 : P_e u \left(\frac{\partial c'_1}{\partial x} + \frac{\partial \bar{c}_1}{\partial x} \right) = \frac{\partial^2 c'_1}{\partial x^2} + \frac{\partial^2 \bar{c}_1}{\partial x^2} + \frac{\partial^2 c'_1}{\partial y^2} + \frac{\partial^2 \bar{c}_1}{\partial y^2} + \frac{\partial^2 c'_2}{\partial z^2} \quad (29)$$

Let us first look at the regions without cells, i.e. $f(c) \equiv 0$. Solving equation (27) we get

$$c_0 = A_1(x, y)z + A_2(x, y), \quad (30)$$

where $A_1(x, y)$ must be 0 to satisfy no flux at $z = 0$ and $z = 1$, so

$$c_0 = A_2(x, y). \quad (31)$$

Since we see that c_0 only depends on x and y , the only z -dependence in (28) is in u and c_1 . In (24) we have an explicit formula for u . Since we found that the y -dependency could be neglected in the center of the box we use the approximation in (20) (where we set $H = 1$ since we are now working with the scaled equations). Then we can integrate the equation with respect to z .

$$\int_0^1 \left(P_e \gamma z(1-z) \frac{\partial c_0}{\partial x} - \frac{\partial^2 c_0}{\partial x^2} - \frac{\partial^2 c_0}{\partial y^2} \right) dz = \int_0^1 \frac{\partial^2 c_1}{\partial z^2} dz$$

$$\frac{P_e \gamma}{6} \frac{\partial c_0}{\partial x} - \frac{\partial^2 c_0}{\partial x^2} - \frac{\partial^2 c_0}{\partial y^2} = 0 \quad (32)$$

By subtracting (32) from (28) we get

$$P_e \gamma \left[z(1-z) - \frac{1}{6} \right] \frac{\partial c_0}{\partial x} = \frac{\partial^2 c_1'}{\partial z^2}. \quad (33)$$

By integrating this equation we find c_1' to be

$$c_1' = P_e \gamma \frac{\partial c_0}{\partial x} \left[-\frac{1}{12} z^4 + \frac{1}{6} z^3 - \frac{1}{12} z^2 + \frac{1}{360} \right]. \quad (34)$$

Inserting this into equation (29), and integrating we get

$$\int_0^1 P_e \gamma z(1-z) \left(P_e \gamma \frac{\partial^2 c_0}{\partial x^2} \left[-\frac{1}{12} z^4 + \frac{1}{6} z^3 - \frac{1}{12} z^2 + \frac{1}{360} \right] + \frac{\partial \bar{c}_1}{\partial x} \right) dz = \int_0^1 \left(\frac{\partial^2 \bar{c}_1}{\partial x^2} + \frac{\partial^2 \bar{c}_1}{\partial y^2} \right) dz \quad (35)$$

which leads to

$$\frac{P_e \gamma}{6} \frac{\partial \bar{c}_1}{\partial x} = \frac{\partial^2 \bar{c}_1}{\partial x^2} + \frac{\partial^2 \bar{c}_1}{\partial y^2} + \frac{(P_e \gamma)^2}{7560} \frac{\partial^2 c_0}{\partial x^2} \quad (36)$$

If we introduce $\bar{c} = c_0 + \epsilon^2 \bar{c}_1$ then equation (32) and (36) can be combined to give

$$\bar{u} \frac{\partial \bar{c}}{\partial x} = \frac{\partial^2 \bar{c}}{\partial x^2} + \frac{\partial^2 \bar{c}}{\partial y^2} + \frac{\bar{u}^2 \epsilon^2}{210} \frac{\partial^2 \bar{c}}{\partial x^2}, \quad (37)$$

where $\bar{u} = \frac{P_e \gamma}{6}$.

Similarly for the areas with cells we find

$$P_e \frac{\partial c_0}{\partial x} = \frac{\partial^2 c_0}{\partial x^2} + \frac{\partial^2 c_0}{\partial y^2} - P_e E_i f(C_r c_0) \quad (38)$$

$$P_e \frac{\partial c_1}{\partial x} = \frac{\partial^2 c_1}{\partial x^2} + \frac{\partial^2 c_1}{\partial y^2} + \frac{P_e^2}{210} \frac{\partial^2 c_0}{\partial x^2} - \frac{P_e^2 E_i}{60} f'(C_r c_0) \frac{\partial c_0}{\partial x} - \epsilon P_e E_i c_1 f'(C_r c_0) \quad (39)$$

where we have defined the Eindhoven number E_i to be

$$E_i = \frac{k\sigma}{CU}. \quad (40)$$

By adding these equations we find

$$P_e \frac{\partial \bar{c}}{\partial x} \left(1 + \frac{\epsilon^2 P_e E_i}{60} f'(C_r \bar{c}) \right) = \frac{\partial^2 \bar{c}}{\partial y^2} + \left(1 + \frac{\epsilon^2 P_e^2}{210} \right) \frac{\partial^2 \bar{c}}{\partial x^2} - P_e E_i f(C_r \bar{c}). \quad (41)$$

This shows us that our problem be reduced to a 2D problem, which we will solve numerically. We that we now get small additional contributions to the advection and diffusion in the x -direction. The last term in (41) is the reduction in concentration due to absorption in the cells.

4 Numerical computations

We created a numerical model to solve the entire 3 dimensional problem of the advection-diffusion equation which governed the concentration (2). However, what we discovered after creating this, was that the 3-dimensional case was more or less redundant. Due to the nature of our problem, we found that by looking at a such small enough box height, this gave almost exactly uniform concentration throughout the z -direction. However, this might not be obvious at first glance, especially when comparing with the velocity field, which varied greatly in the z -direction due to the no-slip condition. In fact: we've allready showed that outside a small boundary layer at $y = 0$ and $y = a$, the velocity field is *only* dependant on z .

4.1 Finite difference discretization

If we look at (4), then we see that c is the only unknown. u is calculated from (24), and moreover is

$$\mathbf{u} = (u(y, z), 0, 0)$$

\Rightarrow

$$\epsilon^2 P_e u(y, z) \frac{\partial c}{\partial x} = \epsilon^2 \left(\frac{\partial^2 c}{\partial x^2} + \frac{\partial^2 c}{\partial y^2} \right) + \frac{\partial^2 c}{\partial z^2} \quad (42)$$

using central difference approximation for first and second order derivatives given as

$$\frac{\partial c}{\partial x} = \frac{c(x+h, y, z) - c(x-h, y, z)}{2h} + \mathcal{O}(h^2) \quad (43)$$

$$\frac{\partial^2 c}{\partial x^2} = \frac{c(x+h, y, z) - 2c(x, y, z) + c(x-h, y, z)}{h^2} + \mathcal{O}(h^2) \quad (44)$$

$$\frac{\partial^2 c}{\partial y^2} = \frac{c(x, y+k, z) - 2c(x, y, z) + c(x, y-k, z)}{k^2} + \mathcal{O}(k^2) \quad (45)$$

$$\frac{\partial^2 c}{\partial z^2} = \frac{c(x, y, z+l) - 2c(x, y, z) + c(x, y, z-l)}{l^2} + \mathcal{O}(l^2) \quad (46)$$

substituting (43)-(46) into (4) we get

$$\begin{aligned} & \epsilon^2 P_e u(y, z) \frac{c(x+h, y, z) - c(x-h, y, z)}{2h} \\ & - \epsilon^2 \left(\frac{c(x+h, y, z) - 2c(x, y, z) + c(x-h, y, z)}{h^2} \right. \\ & \left. + \frac{c(x, y+k, z) - 2c(x, y, z) + c(x, y-k, z)}{k^2} \right) \\ & - \frac{c(x, y, z+l) - 2c(x, y, z) + c(x, y, z-l)}{l^2} = 0 \end{aligned} \quad (47)$$

we discretize the domain in each spatial direction. for each grid point (x_i, y_j, z_p) we obtain a seven point stencil.

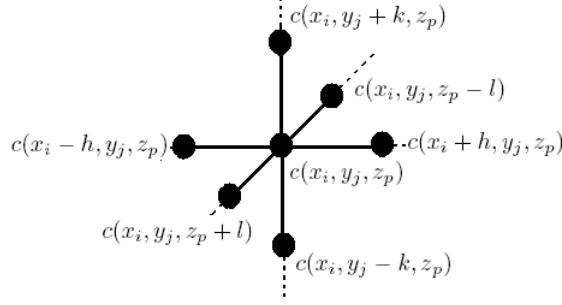


Figure 5: Seven point stencil

and then the discretised equation becomes

$$\begin{aligned}
& \epsilon^2 P_e u(y_j, z_p) \frac{c(x_i + h, y_j, z_p) - c(x_i - h, y_j, z_p)}{2h} \\
& - \epsilon^2 \left(\frac{c(x_i + h, y_j, z_p) - 2c(x_i, y_j, z_p) + c(x_i - h, y_j, z_p)}{h^2} \right. \\
& \quad \left. + \frac{c(x_i, y_j + k, z_p) - 2c(x_i, y_j, z_p) + c(x_i, y_j - k, z_p)}{k^2} \right) \\
& \quad - \frac{c(x_i, y_j, z_p + l) - 2c(x_i, y_j, z_p) + c(x_i, y_j, z_p - l)}{l^2} = 0
\end{aligned} \tag{48}$$

corresponding equation in index notation is given as

$$\begin{aligned}
& \epsilon^2 P_e u_{j,p} \frac{c_{i+1,j,p} - c_{i-1,j,p}}{2h} \\
& - \epsilon^2 \left(\frac{c_{i+1,j,p} - 2c_{i,j,p} + c_{i-1,j,p}}{h^2} + \frac{c_{i,j+1,p} - 2c_{i,j,p} + c_{i,j-1,p}}{k^2} \right) \\
& \quad - \frac{c_{i,j,p+1} - 2c_{i,j,p} + c_{i,j,p-1}}{l^2} = 0
\end{aligned} \tag{49}$$

where i, j, p are index for the grid points in x, y and z direction respectively for example when $x = 0 \Rightarrow i = 1$ and $x = L \Rightarrow i = i_{max}$. Above equation holds for all grid point (x_i, y_j, z_p) .

4.2 Boundary Conditions

We apply no flux condition on the walls $\frac{\partial c}{\partial n} = 0$ of box with an initial concentration $c = f(y, z)$ on the entrance of the wall which is being carry in the x -direction due to the velocity of fluid at the entrance. Along with this we have uniform change of concentration condition at the exit of the box $\frac{\partial^2 c}{\partial x^2} = 0$, which can be interpreted as there is no further change in the concentration due to the velocity conditions at the inlet of the box.

$$\begin{aligned} \frac{\partial c}{\partial n} = 0 \text{ on the following planes } z = 0, z = L, y = 0, y = W. \\ c = f(y, z) \text{ at } x = 0 \text{ and } \frac{\partial^2 c}{\partial x^2} = 0 \text{ at } x = L. \end{aligned}$$

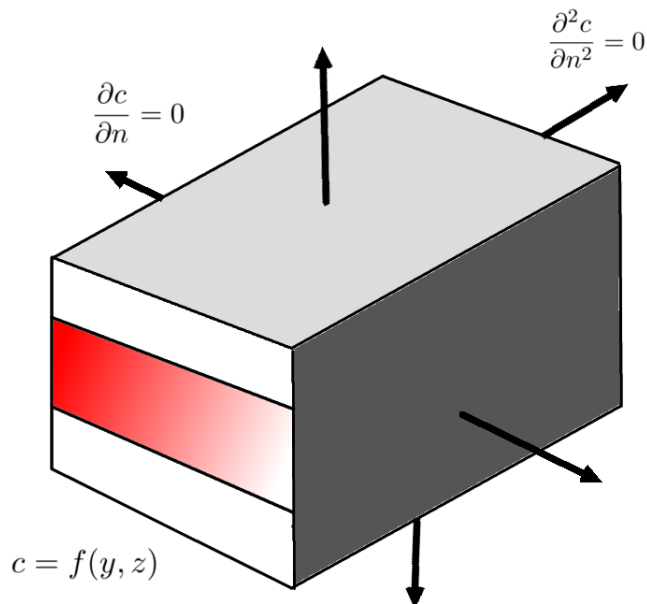


Figure 6: Boundary conditions

The non-homogenous Dirichlet boundary condition at $x = 0$ is in our implementation imposed as

$$c(0, y, z) = f(y, z) = \begin{cases} y & : 1/3 < z < 2/3 \\ 0 & : \text{otherwise} \end{cases} \quad (50)$$

Which is shown in figure 6 as white where the concentration is zero, and increasing to red where the boundary concentration is one. This means that the initial concentration is increasing linearly in y and making a discontinuous jump in the z direction. What we will be focusing on, is the variation of concentration in the z -direction.

We use central difference approximation for $\frac{\partial c}{\partial x}$, $\frac{\partial c}{\partial y}$, $\frac{\partial c}{\partial z}$, and $\frac{\partial^2 c}{\partial x^2}$ to modify (49) in order to find the nodal value of corresponding boundary point. Which gives us following equations at the boundary

$$\begin{aligned}
c_{i-1,j,p} &= c_{i+1,j,p} \\
c_{i,j-1,p} &= c_{i,j+1,p} \\
c_{i,j,p-1} &= c_{i,j,p+1} \\
c_{i+1,j,p} &= 2c_{i,j,p} - c_{i-1,j,p}
\end{aligned} \tag{51}$$

4.3 Grid, and construction of A

The domain nodes are at this moment defined by the three indices i, j, p corresponding to x -, y - and z - position respectively. However for implementation, we will need to map the entire domain into a single array defined by only one index. Thus we create a mapping $\varphi : \mathbb{Z}^3 \rightarrow \mathbb{Z}$ and corresponding inverse φ^{-1} defined by

$$\varphi(i, j, p) = p \cdot NM + j \cdot N + i \tag{52}$$

$$\varphi^{-1}(\alpha) = \begin{cases} \alpha \bmod N \\ \lfloor \frac{\alpha}{N} \rfloor \bmod M \\ \lfloor \frac{\alpha}{NM} \rfloor \end{cases} \tag{53}$$

where N, M is the number of discrete nodes in x - and y -direction respectively. This is also referred to as the natural numbering.

After wrapping up our domain from 3 dimensions into one through φ , we create the stiffness matrix A . Based on our seven point stencil seen in figure 5 we can already see that each row in A will contain 7 nonzero entries, and will in fact due to the natural numbering of our nodes be banded as well.

Without going into too much detail, we created the matrix by filling in each nonzero entry given by (49) taking care at the boundary to satisfy the conditions stated above. While it might have been appropriate at this stage to look into the properties of A on whether it might be symmetric (not obvious due to the boundary conditions) or even positive definite to possibly utilize faster solution algorithms, this was not done. Given the scope of this project, optimized code and fast solvers was not given priority but this might be an issue for further work. To solve the system, we used MATLAB's general solver for linear systems.

4.4 Results

Once we had our numerical implementation up and running, we did several experiments. The first one was to see what kind of behaviour one would expect from the system in all its generality. We set both P_e and ϵ to one, so that every part of (4) had an impact on the solution. What we expected to see in this case, was that the diffusion part of the equation ensured that the concentration would be spread out in all directions, while the advection part would transport the concentration in the positive x direction.

As is clearly seen, this is the case. The concentration is diffused smoothly in the z -direction while also being carried away by the current in the x -direction. Due to our

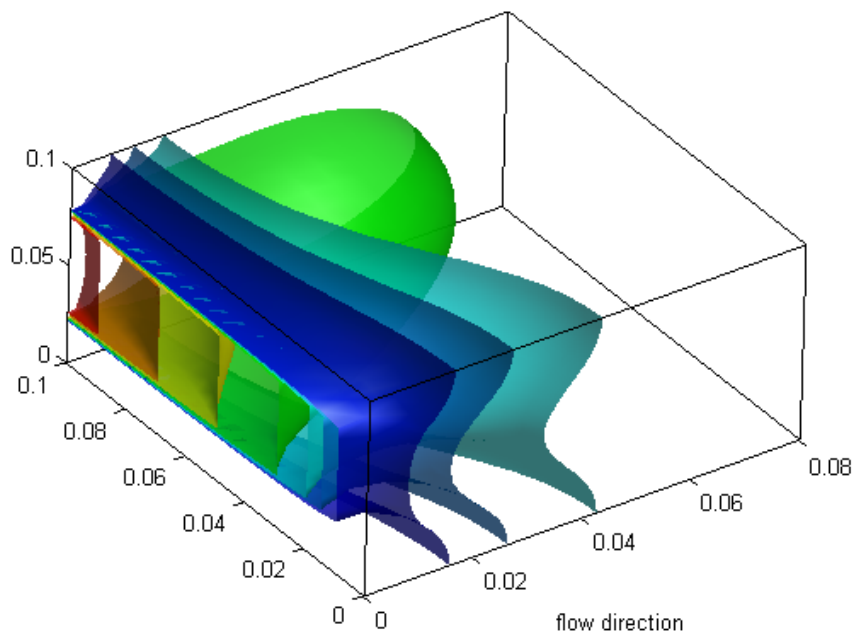


Figure 7: Concentration distribution in a square box

square box, we don't see much of the diffusion in the y -direction, but given a long enough box, this would ultimately result in the concentration being uniform across y .

The next thing we did was to try and set the variables to the problem parameters as given to us in (7).

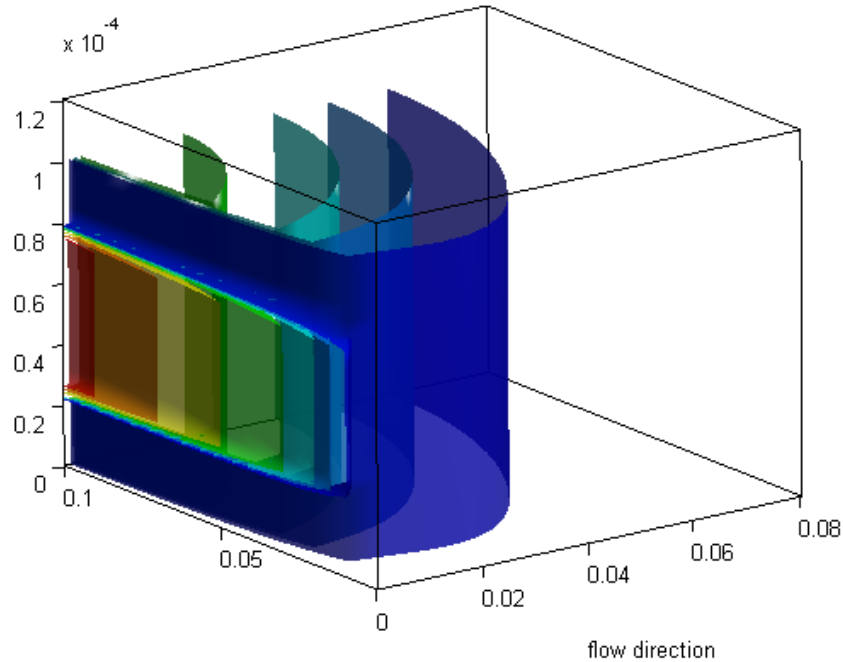


Figure 8: Concentration distribution given problem parameters

What happens now is that the concentration very quickly diffuses throughout the z -direction. Almost instantly after the flow has left the mixer the concentration has spread out enough to make it uniform in z . Recall that we are dealing with a scaled problem, so even if figure 8 appears to be square, it is far from it. Every axis is scaled to be in the interval $(0, 1)$, and for visualization purposes they are not scaled back prior to presentation. This makes it easier to see what is happening in the z -direction.

We did several other experiments as well, but they all supported the same conclusion: the variation of concentration in z is negligible and the problem can safely be approximated as a 2D-problem. This is what we'll consider in the rest of this report.

5 The 2D advection-diffusion case

In this section we will focus on the steady 2D version of the advection-diffusion equation. The transient regime will not be taken into account, since we will allow the system time enough to reach the steady-state. The concentration field c will be regarded as an effectively bidimensional quantity $c = c(x, y)$, and we will neglect the fluid-wall interactions, i.e., we will not include the non-slip effect at the glass plates. We will show that, even for a such crude approximation, it is possible to extract valuable analytical and numerical incite without the need to solve the full 3D problem. It is also worth noting that this 2D simplification is only plausible because the physical system in study is confined in a very narrow gap-space b , where $b/L \ll 1$.

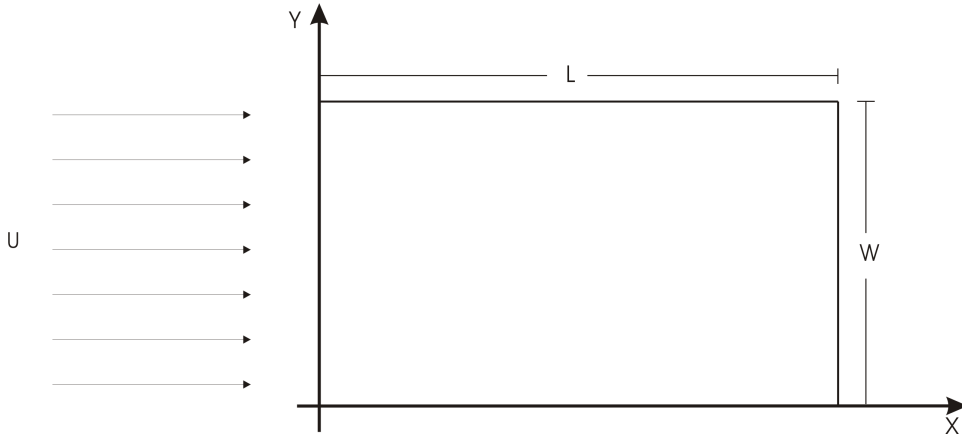


Figure 9: Schematic representation of the interrogator with total length L and width W , subject to a constat input concentration flow in x direction

5.1 Approximate steady-sate solution

Consider an interrogator with total length L and width h , subject to a constant and unitary concentration flow in the x direction, so that $\mathbf{u} = \hat{\mathbf{x}}$ (see Fig 9). The inlet concentration profile is know at $x = 0$ and is only function of y , where $c(0, y) = g(y)$. In this way, if we take the leading order in (4), i.e. $\varepsilon^2 P_e^2 \ll 1$, the non-dimensional advection-diffusion equation can simplified into

$$P_e \frac{\partial c}{\partial x} = \nabla_{\perp}^2 c, \quad (54)$$

where P_e is the Peclet number as before, and ∇_{\perp}^2 denote the two-dimensional Laplacian. Since the concentration field varies more rapidly in the y than x direction, (54) can be further simplified into a heat-equation type

$$\frac{\partial c}{\partial x} = \frac{1}{P_e} \frac{\partial^2 c}{\partial y^2}, \quad (55)$$

where instead of c relaxing in time, the diffusion will make c decay in space (x direction). (55) is subjected to the following boundary conditions : (i) no concentration flux at the wall $\partial c/\partial y = 0$ at $y = 0, W$, and (ii) a known concentration profile $c(0, y) = g(y)$ at $x = 0$.

The solution for (55) admits an analytical form, and it can be easily evaluated using separations of variables. Substituting $c(x, y) = X(x)Y(y)$ into (55) we find

$$P_e \frac{X'}{X} = \frac{Y''}{Y}, \quad (56)$$

where prime denotes its derivative. Since the right hand side depends only on y and the left hand side only on x , both sides are equal to some constant value $-\lambda$. Note that (56) only admits a solution for $\lambda > 0$. Thus, the general solution is given by a linear combination for all λ ,

$$c(x, y) = \sum_{\lambda} e^{-\frac{\lambda^2}{P_e}x} [A_{\lambda} \cos(\lambda y) + B_{\lambda} \sin(\lambda y)]. \quad (57)$$

In order to evaluate the coefficients A_{λ} and B_{λ} , we make use of the specified the boundary conditions. By using the no flux boundary condition, we find $B_{\lambda} = 0$ for all λ , and $\lambda = \frac{n\pi}{W}$. Thus, (57) turns into

$$c(x, y) = \sum_{n=-\infty}^{n=+\infty} A_n e^{-\frac{\lambda^2}{P_e}x} \cos\left(\frac{n\pi y}{W}\right). \quad (58)$$

Now, one needs to specify the input concentration at $x = 0$ so as to evaluate the coefficient A_n . Let's consider a step-function profile

$$g(y) = \begin{cases} 1, & 0 \leq y \leq \frac{W}{2} \\ 0, & \frac{W}{2} < y \leq W \end{cases},$$

so that

$$g(y) = \sum_{n=-\infty}^{n=+\infty} A_n \cos\left(\frac{n\pi y}{W}\right). \quad (59)$$

Using the fact that

$$\int_0^W A_n \cos\left(\frac{n\pi y}{W}\right) \cos\left(\frac{m\pi y}{W}\right) dy = \begin{cases} 0, & \text{if } m \neq n \\ \frac{A_n W}{2}, & \text{if } m = n \neq 0 \\ A_0 W, & \text{if } m = n = 0 \end{cases},$$

the solution for the concentration field is then given by

$$c(x, y) = \frac{1}{2} + \sum_{n \text{ odd}} \left(\frac{2}{n\pi}\right) \sin\left(\frac{n\pi}{2}\right) e^{-\frac{\lambda^2}{P_e}x} \cos\left(\frac{n\pi y}{W}\right), \quad (60)$$

which in an simple analytical formulae for each point in the interrogator.

The most distinguish aspect of the (60) is that $c(x, y)$ has an exponential decay in the x direction, unveiling that the diffusion effect relaxes the concentration very quickly, but still regulated by the Peclet number. As we increase P_e , we decrease the concentration decay rate, since the advection effect starts to contribute more in the dynamics. It is also important to stress the fact that when you look very far in the x direction the diffusion dominates in such a way that the concentration field is constat no matter the value of P_e , i.e, when $x \rightarrow \infty$, $c(x, y) \rightarrow 1/2$. However, it possible to calculate a finite distance from the inlet flow in which the the concentration is almost constant. In this way, we find that the typical length scale is given by

$$L_p = \left(\frac{W}{\pi}\right)^2 P_e, \quad (61)$$

where we used the fact that the fundamental mode ($n = 1$) gives the slowest decay.

In order to gain an overall view of how the diffusion influences the concentration field, we show in Fig. 10 the concentration c , given by (60), as function of x and y for $W = 1$ and $P_e = 100$. It is clear from Fig. 10 how the step-type concentration $g(y)$ decays along the interrogator, giving us a very good physical incite about this system. One can infer that for this low value of P_e , the diffusion effect dominates the system, not allowing the existence of well defined concentration lanes, as is desired. For this task, we predict that one needs to increase more the Peclet number in such a way that the advection effect dominates close to the inlet flow region, allowing us to have concentration lanes along the interrogator with almost constant vales given by the original input concentration at $x = 0$. One can easily see that for $P_e = 100$, only a very small portion of the interrogator still have the original input concentration.

In addition, Fig. 10 also depicts how the contour lines that start from $y = 0.5$, $x = 0$, and extend in to the x direction, eventually reach the wall perpendicularly, due to the no concentration flux condition at the wall. Each contour line defines a region on the interrogator where the concentration will not vary across this area. Fortunately, it is possible to estimate the the contour line shape, for the interrogator region very far from the up/bottom wall, that is $l(x) \ll W/2$, where $l(x)$ represents the distance in the y direction from the middle point ($y = W/2$). In this limit, the variations are very small and can be replaced by the function itself, thus (55) can be written as

$$\frac{P_e}{x} \approx \frac{1}{l^2} \therefore l(x) \approx \sqrt{x/P_e}. \quad (62)$$

(62) give us the typical behavior of the diffusion effect for the region far from the wall. One can see that l scales with \sqrt{x} , which is surprisingly what we can infer from Fig. 10. Note that this is a valuable analytical information, since if we consider a patch of cells that absorb part of the nutrient concentration, (62) will tell us the minimum distance in which we can place consecutive pathes of cells down in the interrogator for a given concentration lane, in order to allow all the pathes to have access to the same nutrient concentration level. One can estimate the x distance along the lane, considering a given cell patches diameter $d = l(x)$.

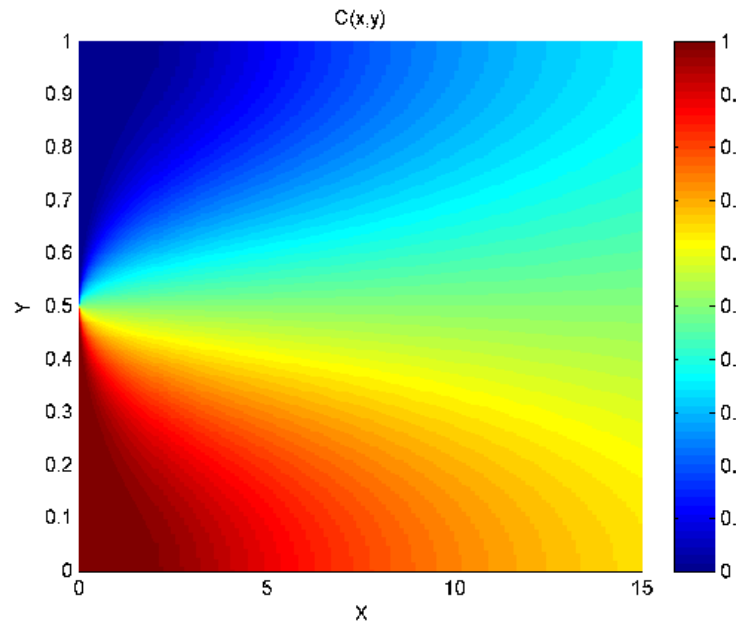


Figure 10: Concentration field c as function of x and y for $W = 1$ and $P_e = 100$.

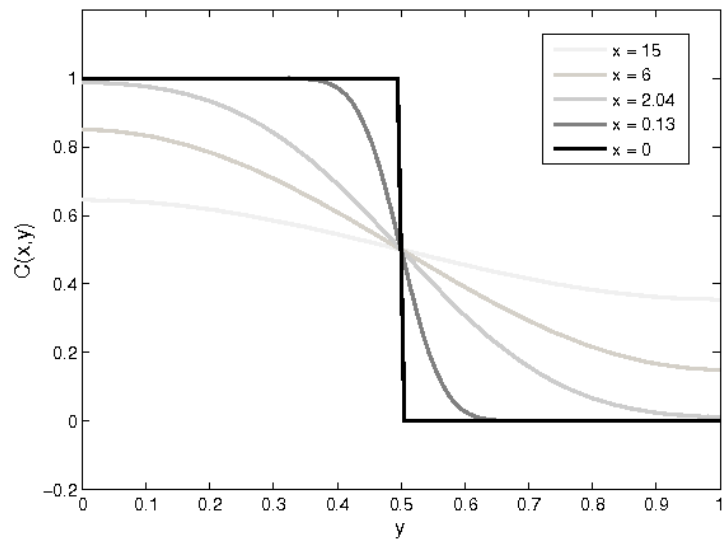


Figure 11: Concentration field c as function of y for various distances in x direction. Here we used $W = 1$ and $P_e = 100$.

Alternatively, it is also possible to visualize in Fig. 11, the diffusion decay behavior for the same set of parameters used in Fig. 10. It is shown in Fig. 11 the concentration c

along y direction for various value of x down in the interrogator. One can see how fast is the concentration decays, as we go further along x , where eventually the concentration field reaches a constant value equal to $1/2$ for large distances from $x = 0$.

It is important to stress the fact that the results obtained in this section was using simplified 2D version for the advection-diffusion equation in the steady-state. All the approximations performed here allowed us to find an exact solution for the problem, and then extract valuable analytical information from the system. Moreover, we were able to find simple length relations and make useful predictions without the need of extensive numerical simulations. However, this simplified version of the problem is not able give us a better understanding about the more complicated situation where the cell absorption interaction is taken into account. In this fashion, it is instructive to solve the full advection-diffusion equation when it have patches of cells absorbing the nutrient in the interrogator.

5.2 Full numerical simulation

In this section we will focus on the full numerical solution of the advection-diffusion equation in the presence or not of absorbing cells in the interrogator. We introduce a reaction rate R due to the patches of cells placed at the bottom of the interrogator, and interacting with the concentration field. In order to simulate its feeding effect, R , which is the uptake rate, is designed to decrease the concentration every time that the nutrient is available close to the cell patch. Thus, the non-dimensional equation can then be written as

$$P_e (\mathbf{u} \cdot \nabla_{\perp})c = \nabla_{\perp}^2 c - D_a R. \quad (63)$$

Here we introduce the Damköhler number given by

$$D_a = \frac{K\sigma L^2}{bc_0 D} \quad (64)$$

where K , σ , c_0 , D are respectively the analyte uptake rate, cells receptor density, initial concentration range and diffusivity of the analyte. All other parameters are as the used in the previous section. In addition, as investigated before, the (4) presents as a good approximation for the full problem, where we used an effective flow that is uniform in z . Following the same idea, we will also focus on the case where the system is driven by a constant and unitary concentration flow in the x direction, that is $\mathbf{u} = \hat{\mathbf{x}}$ as depicted in Fig. 9.

The full numerical solution of (63) was obtained by using Comsol multiphysics, which basically employs the finite difference method, substituting derivatives for its central difference. The mesh points were generated using Comsol built-in adaptative mesh generator in order to obtain good accuracy close to the cell pathes. We also applied the boundary condition as follows: (i) specified concentration profile $g(y)$ at $x = 0$, (ii) no concentration flux condition at the wall, that is at $y = 0, W$ and (iii) open wall at $x = L$.

We start considering the simple case in which no cells are placed in the interrogator, that is $R = 0$ in (63). It is shown in Fig. 12 the numerical solution for the concentration field along the interrogator for various values of P_e , when the input normalized concentration at $x = 0$ is given by

$$g(y) = \begin{cases} 0.125 & : 0 \leq \frac{y}{W} \leq \frac{1}{4}, \\ 0.25 & : \frac{1}{4} < \frac{y}{W} \leq \frac{1}{2}, \\ 0.5 & : \frac{1}{2} < \frac{y}{W} \leq \frac{3}{4}, \\ 1 & : \frac{3}{4} < \frac{y}{W} \leq 1. \end{cases} \quad (65)$$

where L is taken to be unity and the ratio $W/L = 2/5$. As predicted before, in order to obtain well defined concentration lanes down in the interrogator, one need use big values for the Peclet number, since in this way the advection effect will be stronger. However, eventually the diffusion takes place, and then original input concentration start to decay along each lane. Fig. 12 validates the previous result obtained by using simplified equations, and shows us that it is plausible to achieve concentration lanes with a sufficiently high Peclet number.

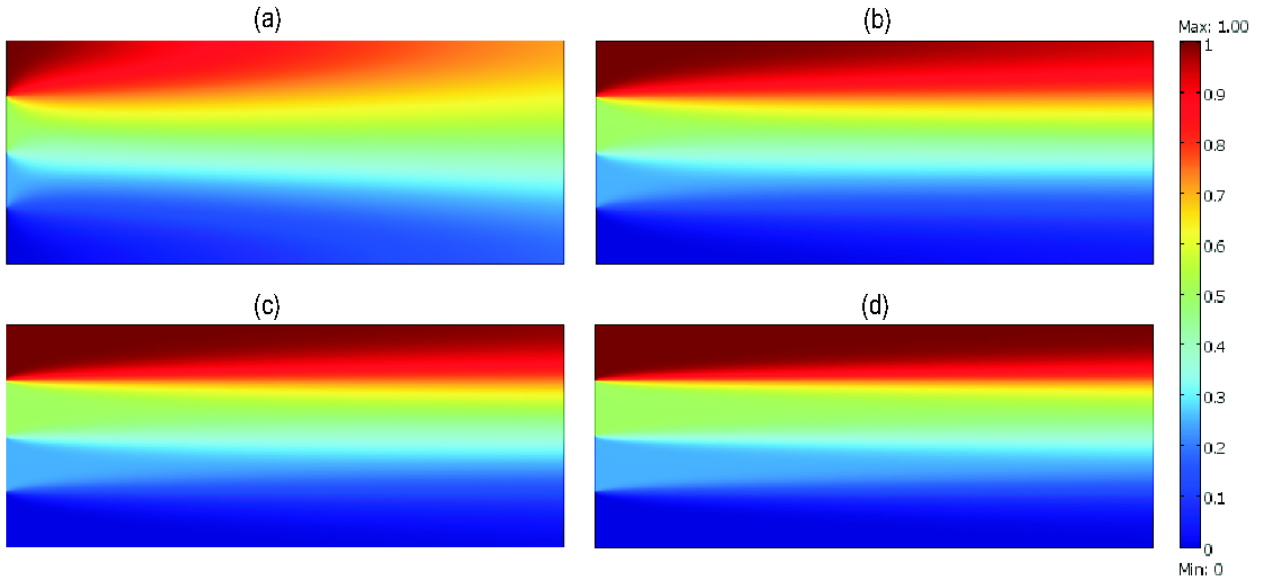


Figure 12: Plots are shown for the concentration field c in the interrogator without any cells with $L = 1$ and $W/L = 2/5$. The normalized input concentration at $x = 0$ is given by (65). (a) $P_e = 100$, (b) $P_e = 500$, (c) $P_e = 1000$ and (d) $P_e = 2000$.

Now, we turn to the effect of the cells interaction in the concentration field. We considered the reaction rate R of each cell as a linear function of the concentration, in this way each cell will only absorb nutrient when it is available nearby. It is depicted in Fig. 13 for a high density of cells in the interrogator for the same values of P_e used in

Fig. 12. For simplicity, we will assume the normalized input concentration as

$$g(y) = \begin{cases} 0 & : 0 \leq \frac{y}{W} \leq \frac{1}{2}, \\ 1 & : \frac{1}{2} < \frac{y}{W} \leq 1. \end{cases} \quad (66)$$

where L is still unity and we kept the same ratio $W/L = 2/5$. It is clear from Fig. 13 that for a such high density of cells, it is not possible to guarantee a specified nutrient concentration for each cell down in the interrogator, even for big values of P_e , as in Fig. 13(d). This is due to the fact that each cell creates a ‘wake’ in the concentration field behind, where continually decrease the nutrient concentration in this direction. Since the advection effect is very strong for $P_e = 2000$, and because the consecutive cell is too close from the previous one, the diffusion effect does not have enough distance to return the concentration to the original concentration for the next cell. This suggest an extra condition to achieve same nutrient concentration levels for each cell, that is the distance between the cells.

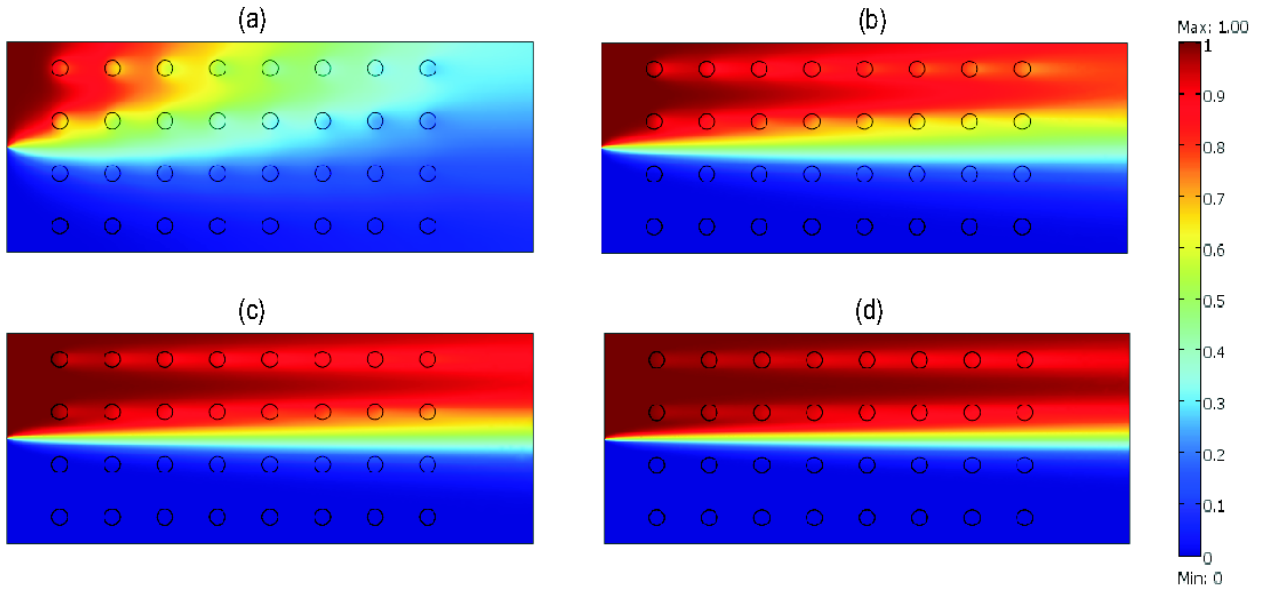


Figure 13: Plots are shown for the concentration field c at the interrogator ($L = 1$ and $W/L = 2/5$) with high density of cells (solid circles). The input concentration at $x = 0$ is given by (66). (a) $P_e = 100$, (b) $P_e = 500$, (c) $P_e = 1000$ and (d) $P_e = 2000$. The reaction rate is a linear function of the concentration $R = c(x, y)$, and $D_a = 20$.

In order to test how the distance between each cell influences the concentration profile, we performed the same numerical solution as presented in Fig. 13, but for a lower cell density and high Peclet number ($P_e = 2000$). It is clear from Fig. 14 how it is possible to regulate the ‘wake’ behind the cell by simply increasing the distance in x between pairs of cells. Now, we allowed the diffusion effect to participate a little bit more in the system by simply increasing the cell distance. In this manner, it is possible to control in a better

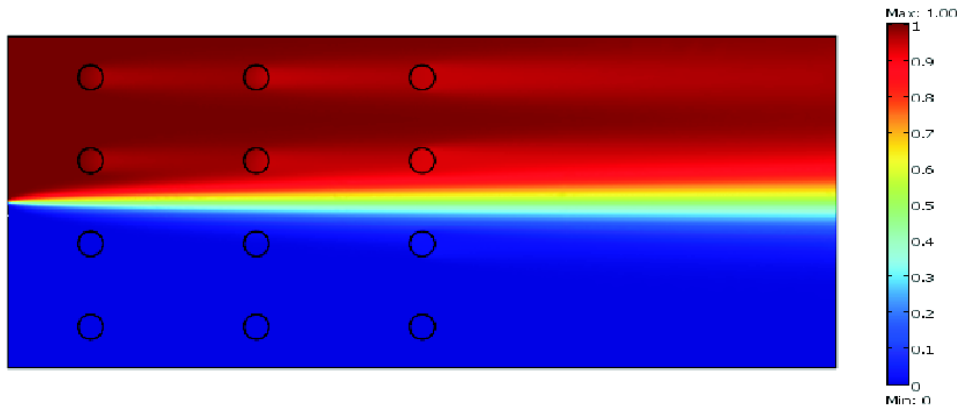


Figure 14: Concentration field c at the interrogator ($L = 1$ and $W/L = 2/5$) with low density of cells (solid circles). The input concentration at $x = 0$ is given by (66), $Pe = 2000$, $R = c(x, y)$ and $Da = 20$.

way the accessed concentration level for each cell by only changing two parameters: (i) the Peclet number and (ii) the cell distance. It is also important to point out that we obtained in the previous section a good estimative for the cell distance given by $x \approx d^2 Pe$, where d represents the cell diameter.

6 Conclusions

In conclusion, by looking at the problems of flow and advection-diffusion in the interrogator separately, we have obtained useful insight into the problem. We have obtained an analytical solution to the flow in the interrogator and the condition under which approximating the flow purely as a function of z is valid. Furthermore, we have shown that the advection-diffusion problem can be reduced to a 2-D problem. Our analysis has also allowed us to determine the conditions for the length of lane mixing and the distance between cell patches. However, in order to be able to say something about inter-lane cell spacing, we would require further information about the mechanisms behind the nutrient uptake into cells.